Radial variation of heat transport in L-mode JET discharges

Radial variation of heat transport in L-mode JET discharges

B.Ph. van Milligen[1], B.A. Carreras[2], E. de la Luna[1] and JET Contributors‡

[1] Laboratorio Nacional de Fusión, CIEMAT, Av. Complutense 40, 28040 Madrid, Spain
[2] Departamento de Física, Universidad Carlos III de Madrid, Av. de la Universidad 30, 28911 Leganés, Madrid, Spain

Abstract. In this paper, we analyze heat transport in the JET tokamak using data from its high resolution ECE diagnostic and analyses based on the transfer entropy. The analysis reveals that heat transport is not smooth and continuous, but is characterized by 'trapping regions' separated by 'minor transport barriers'. Heat may 'jump over' these barriers and when the heating power is raised, this 'jumping' behavior becomes more prominent. To check that our results are relevant for global heat transport, we deduced an effective diffusion coefficient from the transfer entropy results. Both its value and overall radial variation are consistent with heat diffusivities reported in literature. The detailed radial structure of the effective diffusion coefficient was shown to be linked to the mentioned minor transport barriers.

‡ See the author list of X. Litaudon et al 2017 Nucl. Fusion **57** 102001

1. Introduction

The characterization of heat transport in magnetic confinement devices plays a fundamental role in the development of transport models, needed for the design and optimization of future devices in the framework of the search for fusion as an alternative energy source. Electron heat transport has been studied extensively at the European JET tokamak and elsewhere. A prime technique used for this purpose is to generate electron temperature oscillations by modulating a heat source and analyzing the observed propagating heat waves, e.g., using Fourier analysis [1, 2]. Propagating heat (or cold) pulses can also be induced by rapidly cooling the edge plasma.

Spontaneous electron temperature fluctuations can also be used to analyze heat transport. Of course, spontaneous (irregularly occurring) perturbations are not amenable to Fourier analysis, and other techniques, such as conditional averaging, must be used. Recently, we showed how a relatively novel technique (based on the transfer entropy) is capable of extracting useful information from the propagation of small, spontaneous perturbations in the TJ-II and W7-X stellarators [3, 4]. We found that the information obtained is essentially equivalent to the modulation phase (but not the amplitude) obtained from the Fourier analysis, with the advantage of not requiring externally induced perturbations. The propagation of these heat perturbations was found to occur in a stepwise rather than continuous fashion, and we were able to identify both 'trapping zones' and 'radial jumps'. In the cited papers, the spontaneous T_e perturbations arose from the particularities of Electron Cyclotron Resonance (ECR) heating.

At JET, however, this type of heating is not available, and neither are the corresponding perturbations. On the other hand, JET discharges are usually characterized by sawtooth activity in the core region (reconnection events associated with the $q = 1$ rational surface). These events produce a rapid expulsion of heat from the core, and the resulting heat pulses can be analyzed [5, 6] (subject to some caveats, as discussed below). This is the approach taken in the present paper. Thanks to the high spatial resolution of the ECE diagnostic, we obtain detailed radial information on heat transport, and are able to detect the existence of minor transport barriers.

Early work carried out at the RTP tokamak clearly demonstrated the existence of a multiplicity of such transport barriers throughout the plasma [7]. Subsequently, a simplified 'q-comb' model was developed to interpret the observations, based on radially localized reductions of the heat diffusion coefficient, coinciding with low order rational surfaces [8]. The present work confirms that there may be an element of truth in this model, although the appearance of the minor barriers appears to be less systematic than suggested by the q-comb model.

In this framework, it is obligatory to mention Internal Transport Barriers (ITBs), which arise only transiently but are much stronger than the 'minor transport barriers' that are the focus of this paper. In tokamaks, strong ITBs can be established by creating a core reversed magnetic shear region, and the location of the ITB appears

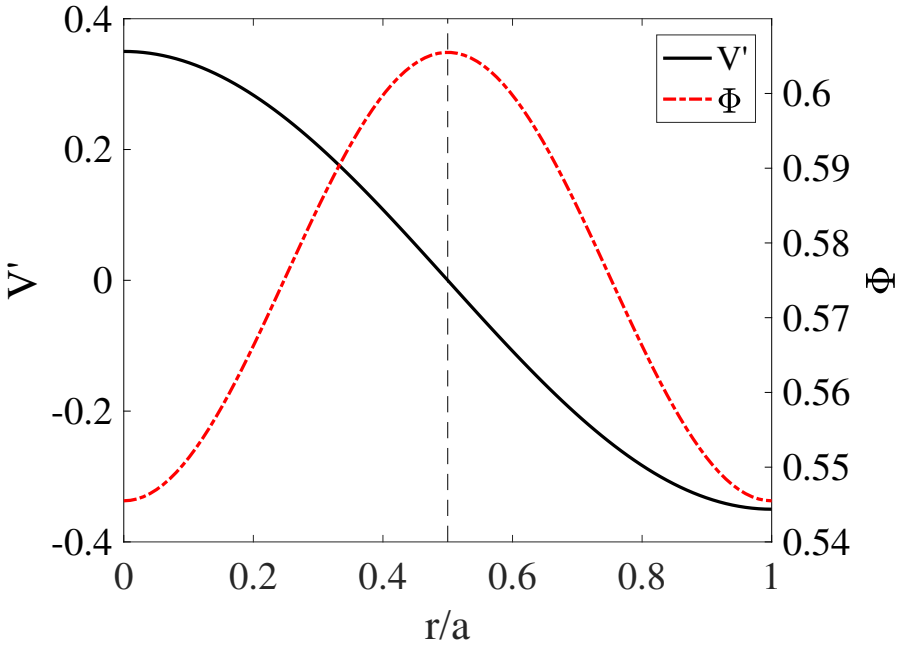

Figure 1. Potential fluctuation (Φ) and shear of the generated flow (V') for a simple nonlinear slab model. The vertical dashed line shows the position of the singular surface.

correlated with integral values of the safety factor, q [9, 10]. The impact of ITBs on heat transport has been studied in some detail at, e.g., Alcator C-Mod [11] and JET [12, 13], showing that the heat diffusivity drops strongly in the ITB region. ITBs have also been obtained and studied in stellarators [14], and here, too, a relationship with the magnetic configuration is suggested.

Theoretically, transport barriers may arise as a consequence of zonal flows generated by turbulence. The mechanics of the interaction between turbulent fluctuations and zonal flows is well understood: fluctuations may generate flows through Reynolds stress [15], and the shear in these flows then suppresses the fluctuations [16]. The complexity of these interactions has been clarified using simplified models [17] and it has been found that shear flow regions are preferentially formed near singular (rational) surfaces.

Fig. 1 shows the radial structure of an electrostatic fluctuation potential near a rational surface, arbitrarily placed at $r/a = 0.5$, and the associated sheared flow in a very simple slab model. This figure is no more than a cartoon, shown here to illustrate the idea of the association between fluctuations, rational surfaces and sheared flow. If the instability eigenfunction Φ is symmetric with respect to the rational surface, the flow shear $|V'|$ will peak off the rational surface, at a distance of the order of the width of the turbulent vortices. Likewise, an antisymmetric eigenfunction will place the flow shear peak at the rational surface. Each type of instability will generate its own structure, possibly modulated by the presence of other structures nearby, and the actual situation

can be much more convoluted. Nevertheless, the central idea is that the sheared flow regions are usually located near singular surfaces. Using a resistive MHD model with tracers, it has been shown [18] that such sheared flow regions act as minor transport barriers, trapping some of the tracers, while other tracers, with higher kinetic energies, perform rapid radial excursions, 'jumping over' the barriers. As the system is driven more strongly (by increasing heating power levels), on average tracers are endowed with higher energies, so that more tracers will be able to 'jump' the minor barriers. This is the mechanism we proposed to explain the deterioration of confinement in the TJ-II stellarator [19].

In this work, we study the propagation of spontaneously generated electron heat pulses using the transfer entropy at JET. The pulses propagate through the various turbulent structures and minor transport barriers. We develop a methodology to identify the location of the main minor transport barriers in the experiment and test the robustness of this identification. In addition, we estimate an effective diffusivity from the TE to quantify heat transport, determine the robustness of the calculation and study the impact of the minor barriers on the radial structure of this effective diffusivity.

Section 2 presents the experiments we have analyzed and the used diagnostics and analysis techniques. Section 3 discusses a set of L-mode discharges, chosen to study the reproducibility of results. Section 4 studies the dependence of results on the heating power level in L-mode. Finally, we discuss the results in Section 5 and draw some conclusions in Section 6.

2. Experimental setup and analysis techniques

The analysis technique used in this paper, based on the transfer entropy, has been very fruitful for the analysis of heat transport in the two stellarators TJ-II [3] and W7-X [4]. In both devices, the technique allowed tracking the radial propagation of heat perturbations, either appearing spontaneously in the power deposition region (as a consequence of the applied ECR Heating) or induced via modulation of the power source. Although, strictly speaking, the transfer entropy quantifies the propagation of information, it was shown that the deduced diffusivity matches the heat diffusivity as measured by more traditional techniques.

The application of this technique at JET presents new challenges. The main challenge is the near omnipresence of sawteeth, produced in the core region due to the fact that typically, $q(0)$ is close to or even below 1. Sawteeth produce a major perturbance of the T_e profile and evidently make it difficult to interpret ECE data in the region inside the sawtooth inversion radius in terms of gradual and smooth outward heat transport. The sawteeth-induced perturbations outside the inversion radius, however, are amenable to such analysis. In this work, all discharges analyzed have sawteeth and our analysis is based on the propagation of the corresponding heat pulses. In this context, we remind the reader of the caveat expressed in Ref. [1]: sawtooth perturbations may affect more than just the T_e profile and may be associated with modifications of

the magnetic geometry due to the core reconnection taking place during the sawtooth crash, leading to the possible misinterpretation of observed T_e perturbations. We note, however, that this misinterpretation mainly refers to the fact that the deduced *value* of the diffusion coefficient may be biased; yet the radial variation of this coefficient can still be fruitfully studied with this method, which is all we intend to do here.

Another challenge is the relatively high magnetic shear of JET, compared with the low-shear stellarator configurations studied in the cited previous work. The added difficulty of the closer spacing of rational surfaces is however partly compensated by the higher radial resolution of the diagnostic system at JET.

H-mode plasmas present further difficulties due to the presence of Edge Localized Modes, among other issues, and we defer the analysis of such discharges to future work.

2.1. Experimental setup

The experiments described here were performed in the JET tokamak (major radius $R_0 = 2.96$ m, minor radius $a = 1$ m). The discharges studied are all in L-mode.

The main diagnostic used is the high resolution ECE radiometer with up to 96 radially distributed channels with a radial separation less than 1 cm [20]. The obtained temperature profiles are cross-calibrated against the Michelson interferometer [21]. The background or electrical noise level in the ECE channels can be estimated from the root mean square (RMS) deviation of the channel in the absence of plasma (typically, this is obtained from data taken after the discharge has terminated). The background noise level varies per channel. In this work, we detect and remove particularly noisy channels.

To infer the approximate position of rational surfaces in the plasma and calculate the approximate value of the safety factor, q, at the measurement positions of the ECE channels, we will make use of the standard EFIT equilibrium reconstruction, based on magnetics only. This calculation is subject to some uncertainty [22], although in the centrally heated, steady state L-mode discharges studied here, the precision should be reasonable in the outer regions of the plasma, while noting that uncertainties increase towards the core. Due to these uncertainties, we will not attempt to identify any of the observed features with specific rational surfaces, even though we will use the EFIT q-profile as guidance for the interpretation. Also, we will compare shots with significantly different q-profiles and compare the shift of rational surfaces in the outer regions of the plasma with the shift of the features we detect.

2.2. The transfer entropy

The Transfer Entropy is a technique from the field of Information Theory [23] that was recently applied for the first time in the context of fusion plasmas [24]. This nonlinear technique measures the 'information transfer' between two signals, is directional, and uses all the information available in the two signals, regardless of amplitude or sign.

The Transfer Entropy is a measure of the causal relation or information flow between two time series. The Transfer Entropy between discretely sampled signals $y(t_i)$ and $x(t_i)$

quantifies the number of bits by which the prediction of the next sample of signal x can be improved by using the time history of not only the signal x itself, but also that of signal y.

In this work, we use a simplified version of the Transfer Entropy:

$$T_{Y\to X} = \sum p(x_{n+1}, x_{n-k}, y_{n-k}) \log_2 \frac{p(x_{n+1}|x_{n-k}, y_{n-k})}{p(x_{n+1}|x_{n-k})}. \quad (1)$$

Here, $p(a|b)$ is the probability distribution of a conditional on b, $p(a|b) = p(a,b)/p(b)$. The probability distributions $p(a, b, c, \ldots)$ are constructed using m bins for each argument, i.e., the object $p(a, b, c, \ldots)$ has m^d bins, where d is the dimension (number of arguments) of p. The sum in Eq. 1 runs over the corresponding discrete bins. The number k can be converted to a 'time lag' by multiplying it by the sampling rate. The construction of the probability distributions is done using 'course graining', i.e., a low number of bins (here, $m = 3$), to obtain statistically significant results. For more information on the technique, please refer to Ref. [24]. The value of the Transfer Entropy T, expressed in bits, can be compared with the total bit range, $\log_2 m$, equal to the maximum possible value of T, to help decide whether the Transfer Entropy is significant or not.

The statistical significance of the Transfer Entropy can be estimated by calculating T for two random (noise) signals [25]. Here, we will be analyzing time intervals with a typical duration of about $2 - 3$ s, corresponding to $N = 2 - 8 \cdot 10^3$ points, depending on the sampling rate, and the statistical significance level of T is of the order of $4 \cdot 10^{-3}$ or lower.

The transfer entropy (TE) has proven useful for the study of heat transport in stellarators [3, 4]. It has been shown that the TE delivers essentially the same information as the phase delay obtained from power modulation experiments [4]. The absence of any information equivalent to the modulation amplitude means that only partial information about the diffusion coefficient of the assumed underlying diffusive transport process is obtained, as a full recovery of the effective diffusion coefficient would require both phase and amplitude [26]. In spite of this important limitation, that should be born in mind in the following, the TE is a powerful technique that provides unprecedented radial detail. This is due to some remarkable properties of the TE. First, it is directional, acting as a filter that preferentially selects information components related to (directional) propagation. Second, unlike linear tools such as the cross correlation or the conditional average, it does not depend on the temporal waveform or even the amplitude of the fluctuations, but merely on the time lag between x and y. This converts the technique in an exquisitely sensitive tool to study the propagation of perturbations in highly non-linear systems (such as fusion plasmas), in which perturbations tend to be deformed or change shape quickly as they propagate.

The TE is calculated between 2 signals, in this case between an ECE channel at a reference position $R_{\rm ref}$, and an ECE channel at another position, R. In Fig. 2a, a typical TE graph is shown for $R_{\rm ref} = 3.30$ m, versus time lag and the R value of the other ECE channels. Typical values of the TE are well above the statistical significance

level (cf. Section 2.2). This example graph shows that the overall transport is outward, as indicated by the white dashed line. The velocity of this propagation is consistent with the typical heat transport coefficients measured in the JET tokamak, as discussed in more detail below. Fig. 2b shows the transfer entropy result for the strictly diffusive propagation of a heat pulse launched at $R = 3.3$ m in a simple one-dimensional heat transport model with a constant diffusion coefficient and no convection. The comparison highlights the contrast between the smooth and continuous propagation of information associated with heat transport in the case of pure diffusion and the complex propagation pattern in the case of the experiment.

We draw attention to the fact that the experimental propagation is modulated radially. There are radial zones where the distribution is broader horizontally than elsewhere, as indicated by white arrows in the figure. We interpret these regions as 'trapping regions', where outward transport is delayed and heat tends to accumulate. Some 'dips' are visible in the propagation plume, e.g., at $R \simeq 3.57$ and 3.66. We note that this behavior, seen here in the JET tokamak, is very similar to observations made in earlier work in stellarators [3, 4], suggesting that this is a universal feature of heat transport in magnetic confinement devices. In the framework of sheared flow models, 'minor transport barriers' are regions where the zonal flow shear is high, shearing apart turbulent eddies and suppressing turbulence (fully or partially); these regions would correspond to the observed 'dips'. The 'trapping regions', however, are zones in-between the minor transport barriers, where turbulence is not suppressed, but turbulent vortices exist. Propagating 'heat particles' would tend to be trapped in these vortices and 'stick' here before traveling on, leading to a broader range of time delays with high TE values. This interpretation in terms of 'minor transport barriers' and 'trapping regions' has been verified by analyzing the behavior of tracers in a resistive MHD turbulence simulation [18].

Fig. 3 shows a few of the T_e time traces around the region of one the the 'dips' of Fig. 2a. There are indications of possible small mode activity (at $R \simeq 3.552$), which could be related to the presence of low order rational surfaces and turbulence at this location. We will return to this issue below.

As in the case shown in Fig. 2a, there may be various simultaneous barriers. To facilitate the study of the observed radial variation, we simply compute the time average of the TE versus radius, shown in Fig. 4 for a few choices of R_{ref}. One specific, deep radial minimum, corresponding to the radial 'dip' in the TE graph of Fig. 2a, has been highlighted by means of a vertical black dashed line. It should be noted that the TE decays gradually towards this deep minimum, so that the minimum does not depend on the data of a single channel, reinforcing its robustness. In addition, one observes there are other local minima, corresponding to even softer barriers. At the reference radius, $R = R_{\mathrm{ref}}$, TE is 0 by definition, so the minima occurring at the various values of R_{ref} are not associated with any barrier and should be ignored.

Fig. 4 clarifies that the locations of the TE minima do not depend on the choice of reference radius, within a reasonable range, but rather are associated with the magnetic

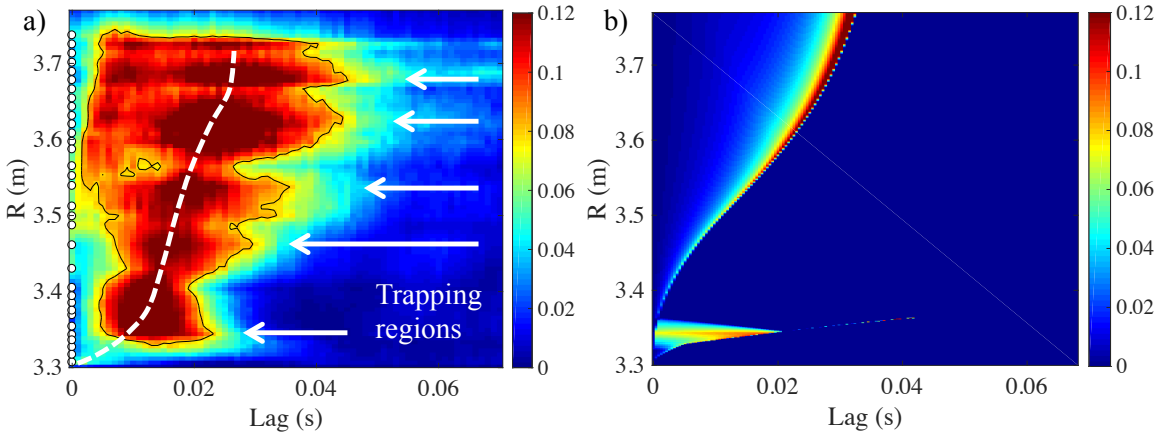

Figure 2. a) Transfer entropy for JET discharge 82292. $R_{\mathrm{ref}} = 3.30$. The color bar indicates the value of TE. White circles indicate the locations of ECE channels. To emphasize the shape of the high TE region, a contour at TE = 0.8 is shown. The white dashed line indicates the overall outward propagation. White arrows indicate 'trapping regions' (see text). b) Example transfer entropy result for the standard diffusive spreading of a heat pulse launched at $R = 3.3$ m, assuming a constant diffusion coefficient and no convection.

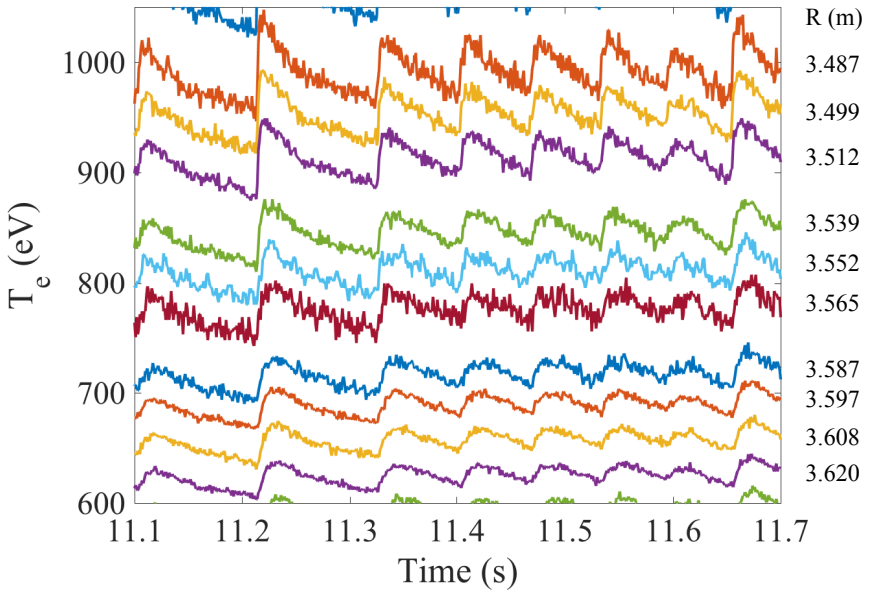

Figure 3. Some time traces of T_e for JET discharge 82292. The radius corresponding to each T_e time trace is indicated on the right.

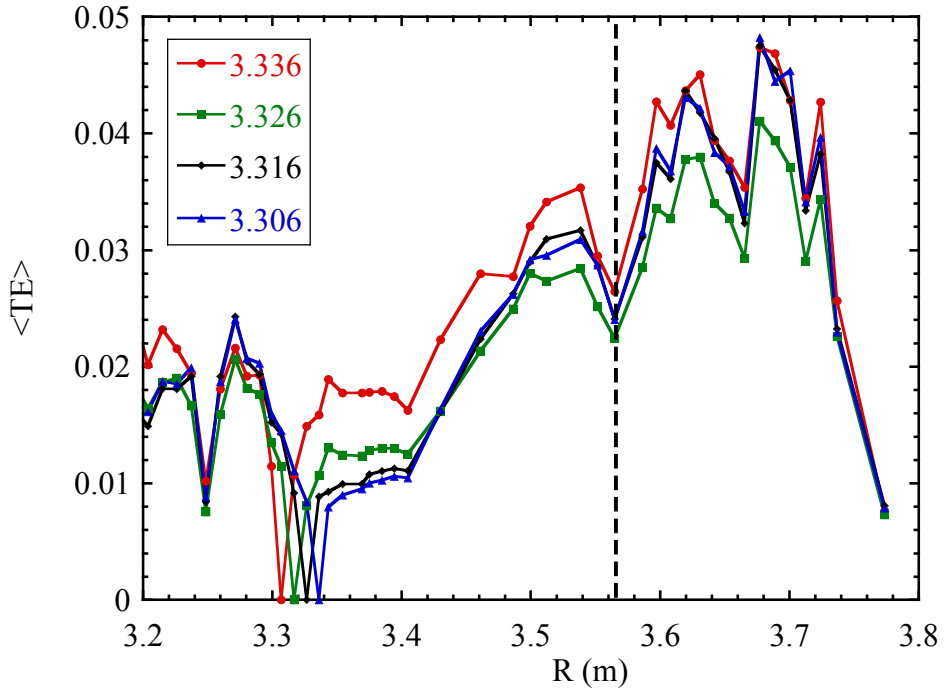

Figure 4. Time average of TE over all time lags $0 \leq \tau \leq 0.2$ s for JET discharge 82292, for a few reference values $R = R_{\rm ref}$, as indicated in the legend.

configuration. Therefore, it is feasible to subject the location of minima in the graphs of $\langle \mathrm{TE} \rangle$ to a statistical analysis, based on the set of all available $R_{\rm ref}$ values for a given discharge. In many cases, we can dispose of between 35 and 65 reference radii. Thus, we can compute how often each local minimum occurs with respect to the total number of reference radii $R_{\rm ref}$ studied, and express it as a percentage. This number is defined as the 'persistence' of any given local minimum.

We then repeat this analysis for different discharges with very similar parameters in order to verify that the locations of the significant (persistent) minima are linked to the plasma configuration. We will present the results of these analyses in the next sections.

2.3. Estimate of effective diffusivity

We will estimate an effective diffusivity from the radial propagation of information [27]. For example, in Fig. 2a, for each available ECE channel (indicated by a white dot at each corresponding value of R), we can estimate the mean time delay $\langle \tau \rangle$ from

$$\langle \tau(R) \rangle = \frac{\int \tau T(R,\tau) d\tau}{\int T(R,\tau) d\tau} \tag{2}$$

Using the equilibrium from EFIT, we can convert the ECE measurement location R to a minor radius value $r = a\sqrt{\Psi_N}$, where Ψ_N is the toroidal flux, normalized to 1 at the

Last Closed Flux Surface. Then, an effective diffusion coefficient can be defined by

$$\langle D \rangle = c \cdot \frac{(r - r_0)^2}{\langle \tau(r) \rangle} \tag{3}$$

The coefficient c appearing in this equation is set at $c = \frac{1}{8}$, corresponding to the 'time to peak' estimate [28], although slightly different values are sometimes also used in literature [5]. Note that this estimate of the effective diffusion coefficient is not very accurate, for two reasons. First, it is not defined for $r = r_0$ as both the enumerator and the denominator of the expression tend to zero, and the radial behavior tends to be dominated by the enumerator $(r-r_0)^2$ for small values of $r-r_0$. Therefore, the extracted diffusion coefficient should not be taken too seriously in the region near the reference position. Second, as discussed above, it is defined exclusively on the basis of the time (or phase) delay, whereas a proper recovery of the underlying effective diffusion coefficient would require information about the perturbation amplitude as well. Nevertheless, it may serve as a means to visualize the radial variation of transport, and in this paper we will use it only for this purpose.

The resulting value $\langle D \rangle$ is the *mean* diffusivity over the interval $[r_0, r]$, which can be expressed as follows:

$$\langle D \rangle_N = \frac{1}{r_N - r_0} \sum_{i=0}^{N-1} (r_{i+1} - r_i) D(r_i), \tag{4}$$

where D is the local diffusivity. Consequently,

$$(r_N - r_0)\langle D \rangle_N - (r_{N-1} - r_0)\langle D \rangle_{N-1} = (r_N - r_{N-1}) D(r_{N-1}), \tag{5}$$

from which the local effective diffusivity, $D(r_{N-1})$ follows. Of course, when $\langle D \rangle$ does not depend strongly on r, the mean diffusivity and the local diffusivity are nearly the same.

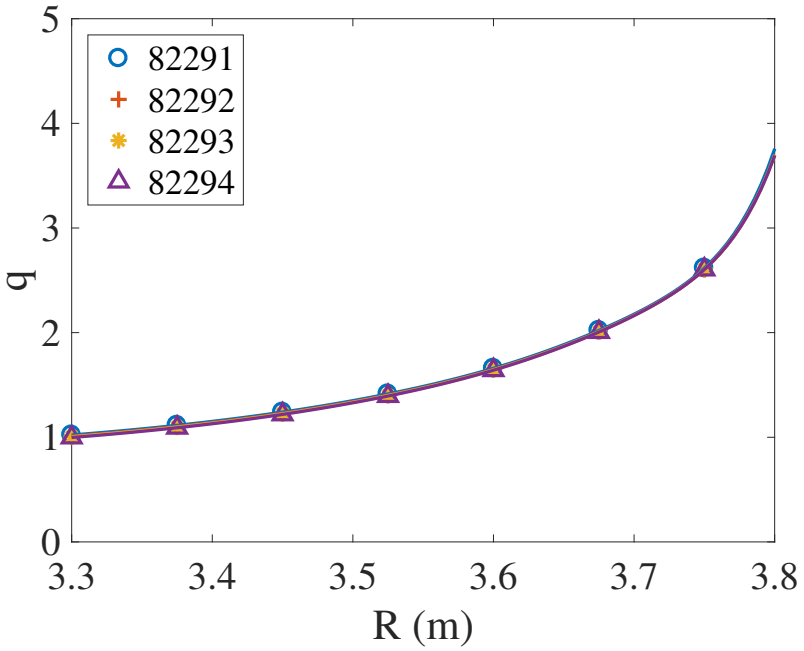

Figure 5. q-profiles for four similar L-mode discharges. Here and in subsequent graphs, the R axis indicates the radial position along the ECE line of sight.

3. Safety factor dependence in L-mode discharges

In this section, we study the L-mode discharges listed in Table 1 [29]. These discharges are heated with Neutral Beam Injection in addition to the standard Ohmic heating of around 1 MW. These discharges are part of the same sequence and they were carried out with under similar conditions and with practically the same q profile (Fig. 5).

Table 1. JET L-mode discharges analyzed

Discharge	Time range (s)	P_{NBI} (MW)	$\overline{n}_e$ (10^{19} m^{-3})
82291	13-16	1	2.7
82292	9-12	1	2.9
82293	9-12	1	2.8
82294	9-12	1	2.8

For each of the discharges in Table 1, we calculated the TE using all possible reference positions R_{ref}. Then we identified the locations of the minima from the time average of TE, $\langle \mathrm{TE} \rangle$, and quantified their persistence, as defined in Section 2.2. The result is shown graphically in Fig. 6. It is clear that positions of many minima are quite persistent within a given shot (reflected by the size and color of the symbols). In addition, the minima are often reproducible from shot to shot. An example of this is the dashed line labelled 2/1, which is associated with a minor barrier in all discharges. Due

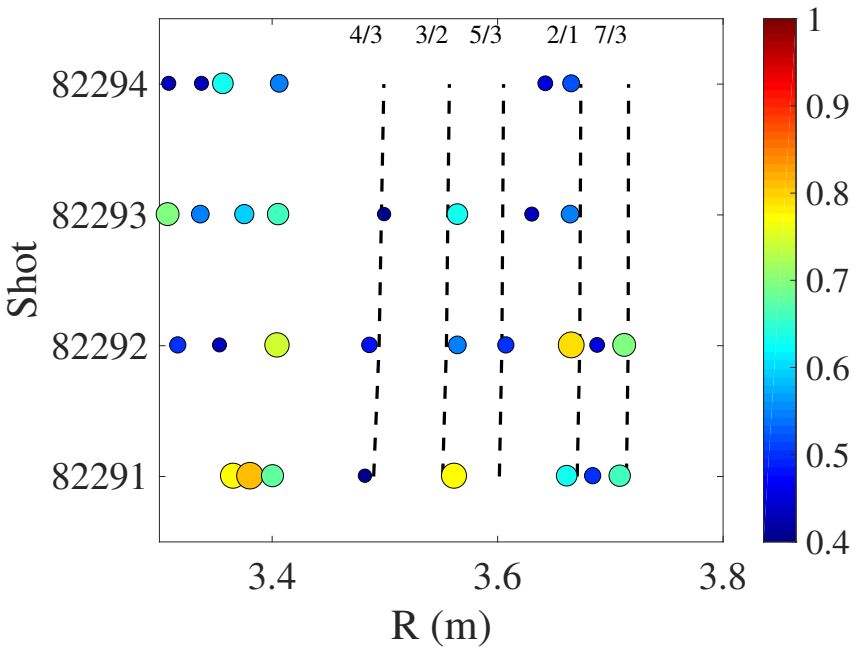

Figure 6. Comparison of the distribution of minima between the four L-mode discharges with a similar q profile and two discharges with different q. The diameter of the circles and their color are proportional to the barrier persistence (minimum value shown: 40 %). Dashed lines indicate the approximate location of a few low order rational surfaces (according to EFIT, having a limited precision), as indicated by the labels at the top of the figure.

to the limited precision of the EFIT estimate of the location of the rational surfaces, we do not assign much importance to the actual value of q indicated by the line label. As argued in the Section 1, the minor barriers do not need to coincide with the locations of rational surfaces. Nevertheless, it should be remembered that part of the deviation between the locations of the minor barriers and the estimated location of the various rational surfaces may be due to imprecisions in the calculation of the latter, noting that this lack of precision increases towards the core (small R).

Fig. 7 shows the mean effective diffusion coefficient for the first four discharges of Table 1 with a similar q profile, calculated according to Eq. (5). The deduced effective diffusivities vary only little between these similar discharges, as indicated by the error bars, suggesting that the method is rather robust. Fig. 8 shows a comparison between the effective diffusivities of two of the shots used to elaborate Fig. 7 and the corresponding barrier persistence. Although both quantities are computed from the TE, the persistence depends on its amplitude and the effective diffusivity on its temporal distribution, hence these two estimates are independent. In a number of cases, the radial structures in D_{eff} are correlated with the positions of the minor barriers, quantified using the persistence statistic: in the top figure, at $r \simeq 0.625$ and 0.725 ($R \simeq 3.56$ and 3.66 m, respectively) and in the bottom figure, at $r \simeq 0.73$ ($R \simeq 3.67$ m).

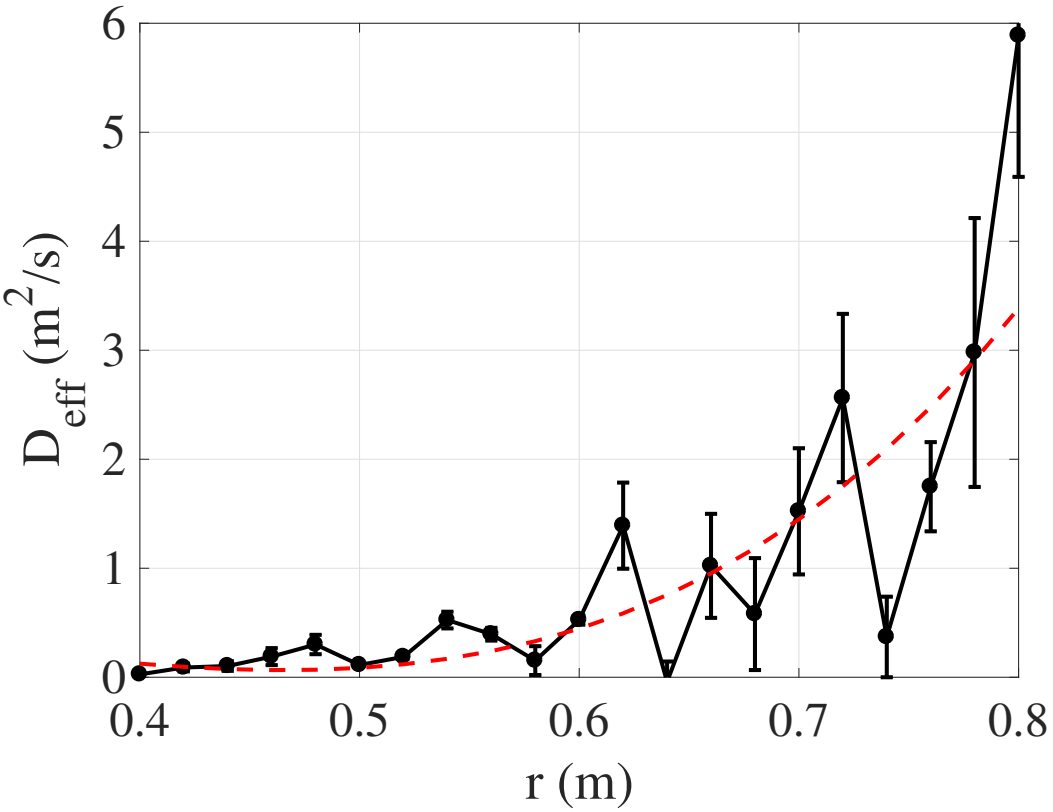

Figure 7. Mean effective diffusion coefficient for the discharges of Table 1 (8229x). Error bars indicate the standard deviation. The red dashed line is a low-order polynomial fit, shown to guide the eye.

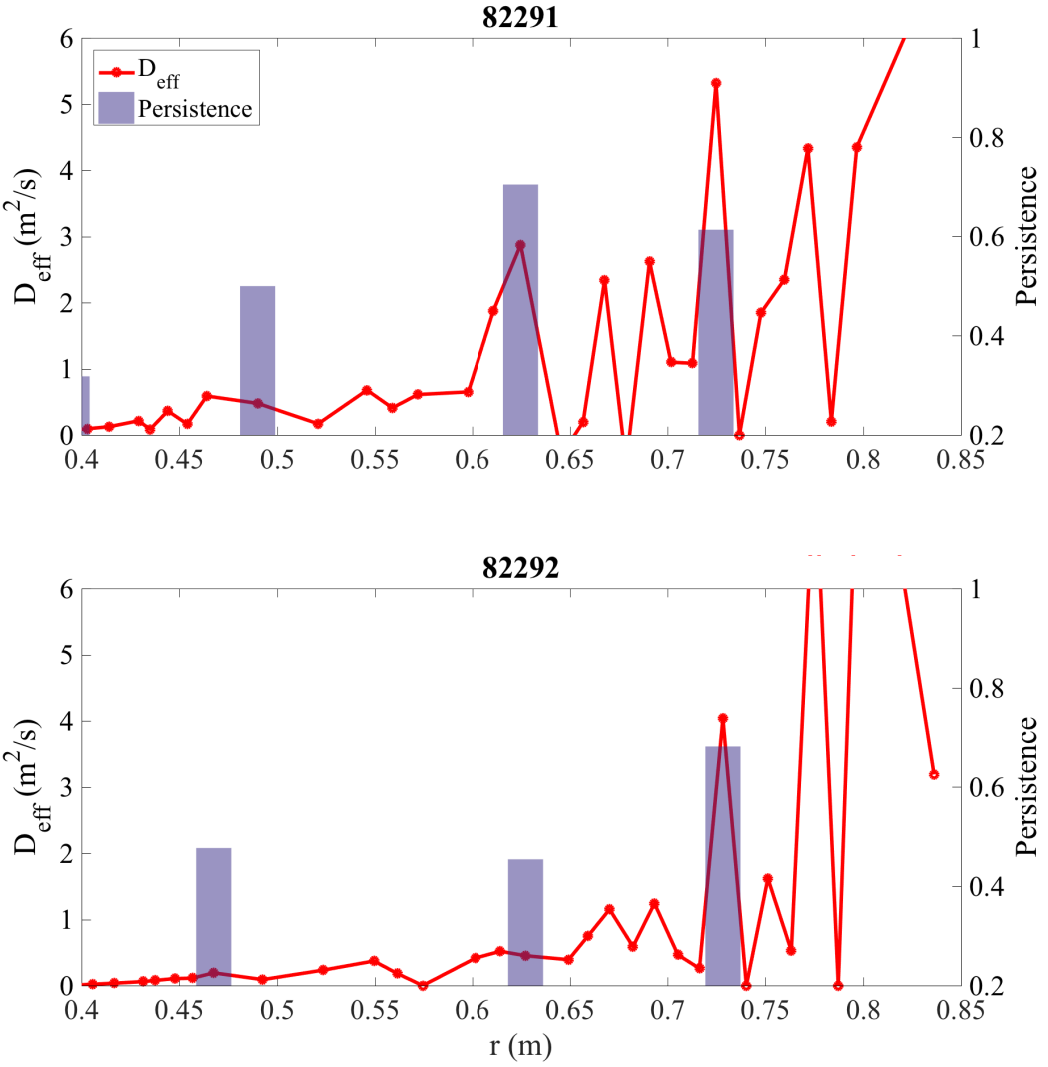

Figure 8. Effective diffusion coefficient and barrier persistence for two similar discharges.

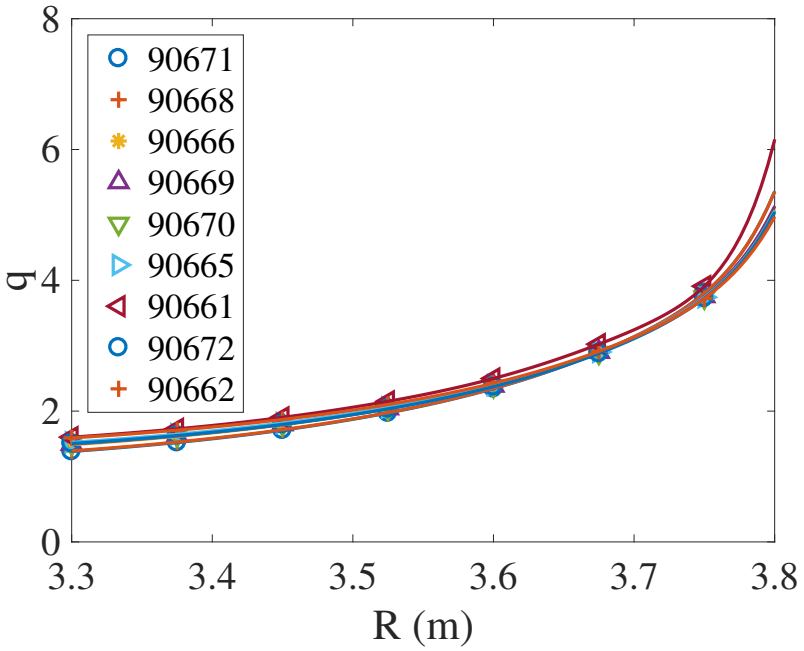

Figure 9. q-profiles of the L-mode power scan.

4. L-mode power scan

The discharges studied in this section are L-mode D plasmas with vacuum toroidal magnetic field $B_T \simeq 3.3$ T, plasma current $I_p \simeq 2$ MA and $q_{95} \simeq 5$ (cf. [30] for more information). The corresponding q-profiles are shown in Fig. 9; they are very similar. The plasmas were heated with Ion Cyclotron Resonance Heating (ICRH) at varying power levels (cf. Table 2). We analyze the time interval $9 \leq t \leq 11$ s, in which the plasmas were roughly in steady state.

Table 2. JET L-mode power scan discharges

Discharge	Power (MW)	$\overline{n}_e$ (10^{19} m^{-3})
90671	4.3	2.7
90668	4.4	2.7
90666	6.8	2.6
90669	7.0	2.6
90670	7.6	2.6
90665	7.7	2.5
90661	7.7	2.5
90672	8.0	2.5
90662	8.9	2.6

An example T_e profile is shown in Fig. 10. The ECE measurements are only reliable

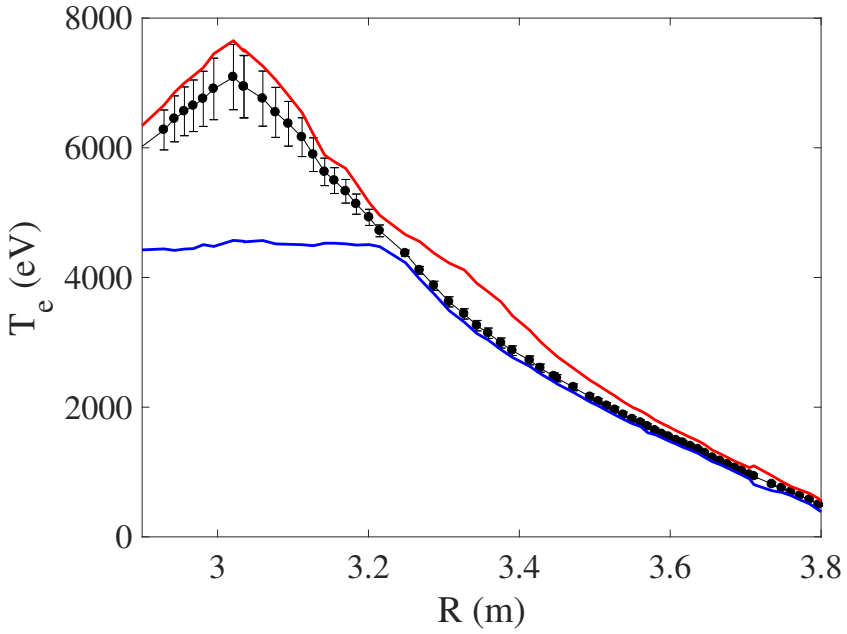

Figure 10. Black dots: ECE T_e-profile of a discharge of the power scan (90672), averaged over the time window of interest. The bars shown indicate the variance of T_e in this time window, not its error. Upper continuous red line: maximum T_e; bottom continuous blue line: minimum T_e over the time window.

for $R < 3.8$; at higher radii, the signal obtained no longer represents a local temperature measurement (due to small optical depth), and the corresponding channels are not considered in the analysis here. The sawtooth region extends up to about $R \simeq 3.22$, while our analyses focus on the heat pulse propagation region $R > 3.3$.

Fig. 11 shows a comparison of the transfer entropy obtained for two discharges from the power scan of Table 2. There are some interesting similarities, such as the 'dip' (barrier) occurring near $R \simeq 3.73$ m. Be that as it may, the difference that we consider most significant is that the propagation in the high-power case seems to be faster (time lags are shorter) and able to 'jump over' the barrier to a larger degree, penetrating further into the edge plasma region. This behavior is consistent with earlier observations made on TJ-II [19].

Next, we calculate the local effective diffusivity using Eq. 3 and Eq. 5 for a few of the discharges. The diffusivity increases with increasing heating power, consistent with power degradation, cf. Fig. 12.

Applying the algorithm to determine the persistence of the local minima of $\langle \mathrm{TE} \rangle$, described in Section 2.2, we obtain Fig. 13. The location of some rational surfaces according to the EFIT reconstruction are indicated; again, due to the limited precision of the equilibrium reconstruction, we do not assign much significance to the indicated rational values, which are merely shown to guide the eye; but we do consider the shot-to-shot variation significant. The barrier near the dashed line labeled 3/1 occurs very systematically for nearly all power levels. Barriers near the line labeled 7/3 follow the

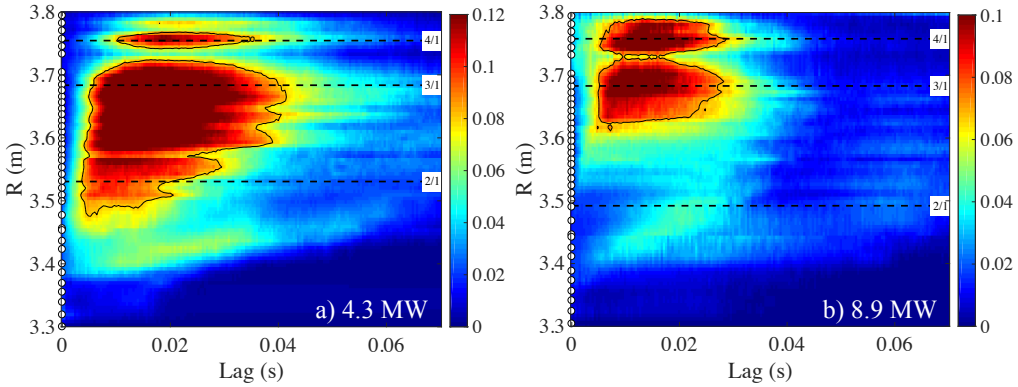

Figure 11. Comparison of transfer entropy between two discharges from the power scan (Table 2), calculated with $R_{\mathrm{ref}} = 3.3$ m and a very different power level (as indicated).

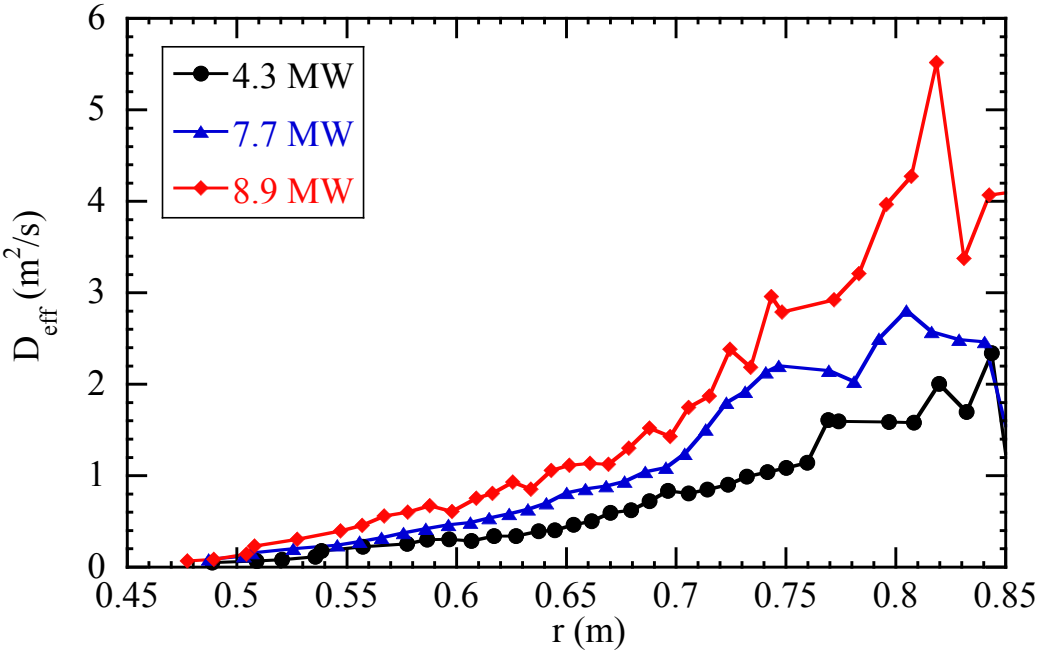

Figure 12. Dependence of effective diffusion on heating power.

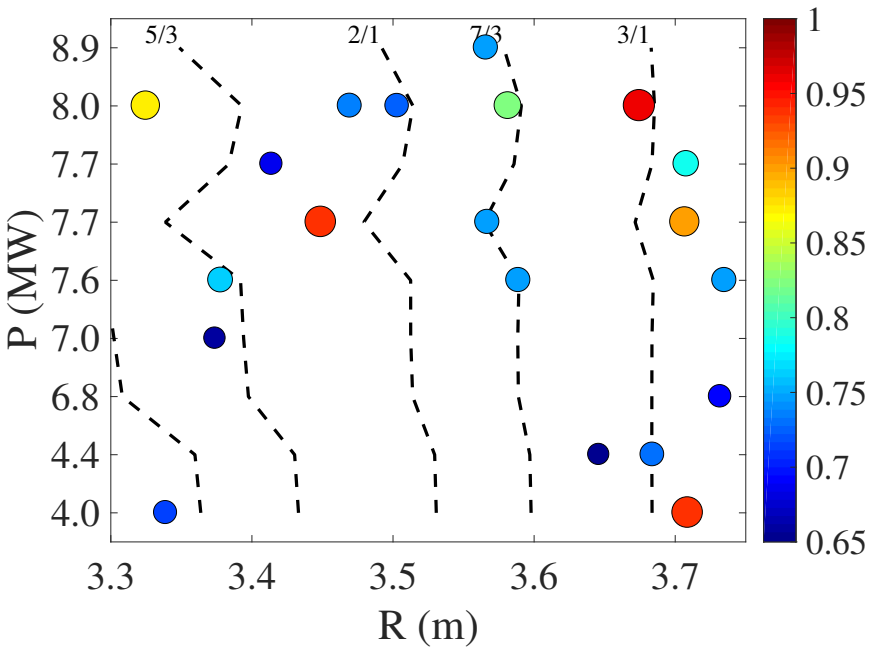

Figure 13. The locations of persistent minor transport barriers. The left axis indicates the power of each discharge listed in Table 2. The diameter of the circles and their color are proportional to the barrier frequency (minimum value shown: 65 %). Dashed lines indicate the approximate location of a few low order rational surfaces (according to EFIT, having a limited precision), as indicated by the labels at the top of the figure.

small variation in its position closely for higher power levels. In the interior of the plasma ($R < 3.6$), one observes that the density of barriers has a tendency to increase as the power level is increased.

Fig. 14 shows the effective diffusion coefficient and the persistence for three discharges at different heating levels. Again, the radial structures seen in the effective diffusion coefficient sometimes appear related to the location of persistent minor transport barriers: namely, at $r \simeq 0.76, 0.83$ (top figure), at $r \simeq 0.7, 0.77, 0.84$ (middle figure), and at $r \simeq 0.745, 0.83$ (bottom figure). The radial resolution and the available statistics are insufficient to determine whether a high persistence systematically corresponds to a low effective diffusivity, as one might expect.

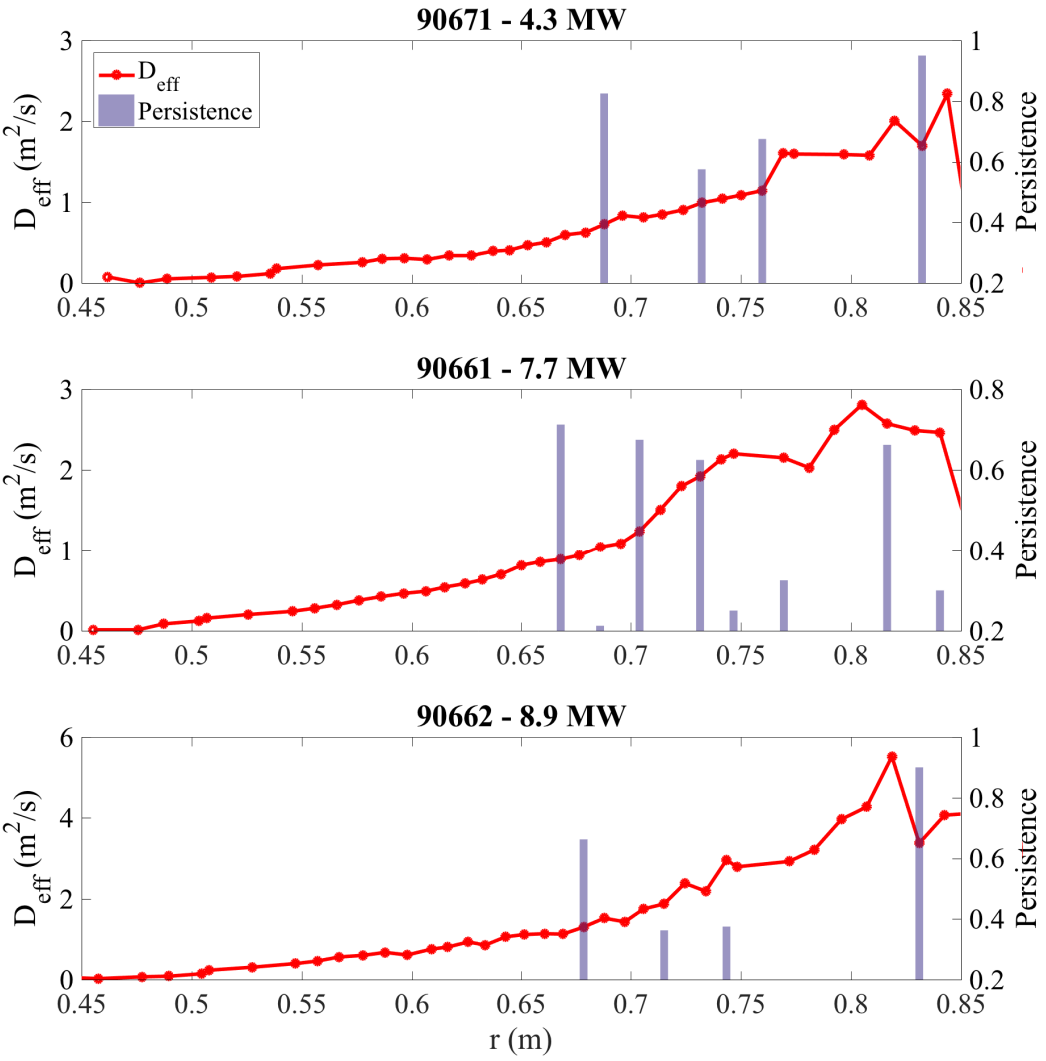

Figure 14. Minor transport barrier frequency and effective diffusion coefficient.

5. Discussion

In this work, we study the propagation of electron temperature perturbations through the plasma of the JET tokamak, in the region between the sawtooth inversion radius and the edge. For this purpose, we make use of data obtained by the ECE radiometer and apply a relatively new analysis technique (based on the transfer entropy) [3, 4]. The combination of the high radial resolution of the diagnostic and the powerful discriminatory capacity of this non-linear analysis technique to follow the propagation of perturbations provides a view of radial heat transport with unprecedented detail.

Using a simple method to estimate an effective radial heat diffusion coefficient from the transfer entropy results (Eq. 5), we find that the deduced effective diffusion coefficient is compatible with typical values of the electron heat diffusion coefficient in JET discharges published elsewhere [1]. Even so, this effective diffusion coefficient has only a limited precision, so we mainly use it to facilitate understanding of the variation of transport with local and global conditions. The variation of the effective heat diffusion with heating power (Fig. 12) is compatible with the commonly observed power degradation effect [31]. These results show that the transfer entropy offers an interesting method to study heat transport, in spite of the fact that it really measures the propagation of 'information' rather than 'heat'. The latter is in agreement with earlier findings [3, 4].

The transfer entropy graph displaying the propagation of information from a reference position R_{ref} was found to exhibit radial 'dips' and 'trapping regions' (Fig. 2a). The 'dips' are considered 'minor transport barriers', whereas the 'trapping regions' are located nearby. In Section 1, it was suggested that the minor transport barriers are likely associated with (low order) rational surfaces, based also on previous numerical studies [18].

The statistics of the occurrence of the 'dips' or minor transport barriers was studied by detecting local minima of the time-average of the transfer entropy, $\langle \mathrm{TE} \rangle$. In a given discharge, the TE was calculated for many values of the reference radius, R_{ref}, and the persistence of local minima in $\langle \mathrm{TE} \rangle$ was calculated. This persistence is taken to be a quantifier of the strength of the minor transport barriers. In a set of similar L-mode discharges, it was found that the pattern of barriers persisted across 4 discharges, confirming the robustness of the method (cf. Fig. 6). Thus, it was shown that the minor transport barriers are associated with rational surfaces, even though we generally prefer to refrain from identifying specific rational surfaces with the detected transport barriers, due to the uncertainties surrounding the reconstruction of the q-profile.

In a second set of L-mode discharges, having similar q-profiles but different heating power levels, it was found that the edge minima of $\langle \mathrm{TE} \rangle$ persisted across discharges and moved radially along with the estimated locations of the rational surfaces, whereas the core minima increased in frequency as power was increased (cf. Fig. 13). This suggests that the minor transport barriers require a certain level of drive (local gradient, induced by heating power) to be established.

In both sets of discharges, the radial variations of the effective diffusion coefficients appear to be linked to the presence of minor transport barriers, as quantified using their degree of persistence (cf. Figs. 8 and 14).

Note that the existence of minor transport barriers does not contradict the global confinement scaling. Comparing different heating levels, it was observed that transport has an increased tendency to 'jump' over the minor barriers as power is increased, cf. Fig. 11. This observation matches the conclusions from earlier work at the TJ-II stellarator and may provide an interesting new viewpoint for understanding the phenomenon of power degradation [19].

6. Conclusions

We have used the high resolution ECE diagnostic and the transfer entropy to detect minor transport barriers in JET L-mode discharges with good radial resolution. This approach offers a new method to study heat transport in magnetically confined plasmas. We have shown that the transport of heat is not smooth and continuous; instead, there are 'trapping regions' separated by 'minor transport barriers'. Heat may 'jump over' these barriers, and when heating power is increased, this 'jumping' behavior becomes more prominent.

By analyzing a set of similar discharges, we show that the method of detecting minor transport barriers is effective and robust. The minor barriers appear to be associated with low order rational surfaces and change position as the q-profile changes. It was also possible to extract an effective diffusion coefficient from the transfer entropy results. The effective diffusion coefficient values and their overall radial variation are consistent with values reported in literature for JET. The detailed radial variation displays structures, associated with local variations of heat transport, that are linked to the detected minor transport barriers.

In a series of L-mode discharges with varying heating power levels, the effective diffusivity changes consistently with the typical power degradation effect observed in magnetic confinement devices. The mechanism underlying this deterioration of confinement may be associated with the increased intensity of the 'jumping' effect observed. This may be an interesting observation in the framework of the effort to understand the mechanisms underlying power degradation in fusion plasmas. It remains to be seen if these minor transport barriers, which are the product of self-regulating mechanisms in the plasma, can be manipulated in any fruitful way.

Acknowledgements

The authors thank E.R. Solano for constructive comments. Research sponsored in part by the Ministerio de Economía y Competitividad of Spain under project Nr. ENE2015-68206-P. This work has been carried out within the framework of the EUROfusion Consortium and has received funding from the Euratom research and training programme 2014-2018 and 2019-2020 under grant agreement No 633053. The views and opinions expressed herein do not necessarily reflect those of the European Commission.

References

[1] P. Mantica and F. Ryter. Perturbative studies of turbulent transport in fusion plasmas. *Comptes Rendus Physique*, 7(6):634, 2006. doi:10.1016/j.crhy.2006.06.004.

[2] M. van Berkel, H.J. Zwart, N. Tamura, G.M.D. Hogeweij, S. Inagaki, M.R. de Baar, and K. Ida. Explicit approximations to estimate the perturbative diffusivity in the presence of convectivity and damping. I. Semi-infinite slab approximations. *Phys. Plasmas*, 21(11):112507, 2014. doi:10.1063/1.4901309.

[3] B.Ph. van Milligen, J.H. Nicolau, L. García, B.A. Carreras, C. Hidalgo, and the TJ-II Team. The impact of rational surfaces on radial heat transport in TJ-II. *Nucl. Fusion*, 57(5):056028, 2017. doi:10.1088/1741-4326/aa611f.

[4] B.Ph. van Milligen, U. Hoefel, J.H. Nicolau, M. Hirsch, L. García, B.A. Carreras, C. Hidalgo, and the W7-X Team. Study of radial heat transport in W7-X using the transfer entropy. *Nucl. Fusion*, 58(7):076002, 2018. doi:10.1088/1741-4326/aabf5d/meta.

[5] E.D. Fredrickson, J.D. Callen, K. McGuire, J.D. Bell, R.J. Colchin, P.C. Efthimion, K.W. Hill, R. Izzo, D.R. Mikkelsen, D.A. Monticello, V. Paré, G. Taylor, and M. Zarnstorff. Heat pulse propagation studies in TFTR. *Nucl. Fusion*, 26:849, 1986. doi:10.1088/0029-5515/26/7/002.

[6] N.J. Lopes Cardozo. Perturbative transport studies in fusion plasmas. *Plasma Phys. Control. Fusion*, 37:799, 1995. doi:10.1088/0741-3335/37/8/001.

[7] N.J. Lopes Cardozo, G.M.D. Hogeweij, M. de Baar, C.J. Barth, M.N.A. Beurskens, F. De Luca, A.J.H. Donné, P. Galli, J.F.M. van Gelder, G. Gorini, B. de Groot, A. Jacchia, F.A. Karelse, J. de Kloe, O.G. Kruijt, J. Lok, P. Mantica, H.J. van der Meiden, A.A.M. Oomens, Th. Oyevaar, F.J. Pijper, R.W. Polman, F. Salzedas, F.C. Schüller, and E. Westerhof. Electron thermal transport in RTP: filaments, barriers and bifurcations. *Plasma Phys. Control. Fusion*, 39:B303, 1997. doi:10.1088/0741-3335/39/12B/023.

[8] A.M.R. Schilham, G.M.D. Hogeweij, and N.J. Lopes Cardozo. Electron thermal transport barriers in RTP: experiment and modelling. *Plasma Phys. Control. Fusion*, 43:1699, 2001. doi:10.1088/0741-3335/43/12/305.

[9] E. Joffrin, C.D. Challis, G.D. Conway, X. Garbet, A. Gude, S. Günter, N.C. Hawkes, T.C. Hender, D.F. Howell, G.T.A. Huysmans, E. Lazzaro, P. Maget, M. Marachek, A.G. Peeters, S.D. Pinches, S.E. Sharapov, and JET-EFDA contributors. Internal transport barrier triggering by rational magnetic flux surfaces in tokamaks. *Nucl. Fusion*, 43(10):1167, 2003. doi:10.1088/0029-5515/43/10/018.

[10] F. Militello, M. Romanelli, J.W. Connor, and R.J. Hastie. Generation of zonal perturbations and transport barriers in plasmas. *Nucl. Fusion*, 51:033006, 2011. doi:10.1088/0029-5515/51/3/033006.

[11] S.J. Wukitch, R.L. Boivin, P.T. Bonoli, C.L. Fiore, R.S. Granetz, M.J. Greenwald, A.E. Hubbard, I.H. Hutchinson, Y. In, J. Irby, Y. Lin, E.S. Marmar, D. Mossessian, M. Porkolab, G. Schilling, J.E. Rice, J.A. Snipes, S.M. Wolfe, and Alcator C-Mod group. Double transport barrier experiments on Alcator C-Mod. *Phys. Plasmas*, 9:2149, 2002. doi:10.1063/1.1467347.

[12] P. Mantica, G. Gorini, F. Imbeaux, J. Kinsey, Y. Sarazin, R. Budny, I. Coffey, R. Dux, X. Garbet, L. Garzotti, C. Ingesson, M. Kissick, V. Parail, C. Sozzi, A. Walden, and contributors to the EFDA-JET Workprogramme. Perturbative transport experiments in JET low or reverse magnetic shear plasmas. *Plasma Phys. Control. Fusion*, 44:2185, 2002. doi:10.1088/0741-3335/44/10/308.

[13] A. Marinoni, P. Mantica, D. Van Eester, F. Imbeaux, M. Mantsinen, N. Hawkes, E. Joffrin, V. Kiptily, S. D. Pinches, A. Salmi, S. Sharapov, I. Voitsekhovitch, P. de Vries, K. D Zastrow, and JET-EFDA contributors. Analysis and modelling of power modulation experiments in JET plasmas with internal transport barriers. *Plasma Phys. Control. Fusion*, 48:1469, 2006. doi:10.1088/0741-3335/48/10/002.

[14] A. Fujisawa. Transport barriers and bifurcation characteristics in stellarators. *Plasma Phys.*

Control. Fusion, 44:A1, 2002. doi:10.1088/0741-3335/44/5A/301.

[15] B.A. Carreras, V.E. Lynch, and L. García. Electron diamagnetic effects on the resistive pressure-gradient-driven turbulence and poloidal flow generation. *Phys. Plasmas*, 3:1438, 1991. doi:10.1063/1.859709.

[16] H. Biglari, P.H. Diamond, and P.W. Terry. Influence of sheared poloidal rotation on edge turbulence. *Phys. Plasmas*, 2:1, 1990. doi:10.1063/1.859529.

[17] P.H. Diamond, Y.-M. Liang, B.A. Carreras, and P.W. Terry. Self-regulating shear flow turbulence: a paradigm for the L to H transition. *Phys. Rev. Lett.*, 72:2565, 1994. doi:10.1103/PhysRevLett.72.2565.

[18] L. García, B.A. Carreras, and L. Llerena. Relation of plasma flow structures to passive particle tracer orbits. *Nucl. Fusion*, 57:116013, 2017. doi:10.1088/1741-4326/aa7e0b.

[19] B.Ph. van Milligen, B.A. Carreras, C. Hidalgo, Á. Cappa, and the TJ-II Team. A possible mechanism for confinement power degradation in the TJ-II stellarator. *Phys. Plasmas*, 25:062503, 2018. doi:10.1063/1.5029881.

[20] E. de la Luna, J. Sánchez, V. Tribaldos, JET-EFDA contributors, G. Conway, W. Suttrop, J. Fessey, R. Prentice, C. Gowers, and J.M. Chareau. Electron cyclotron emission radiometer upgrade on the Joint European Torus (JET) tokamak. *Rev. Sci. Instrum.*, 75:3831, 2004. doi:10.1063/1.1781376.

[21] S. Schmuck, J. Fessey, T. Gerbaud, B. Alper, M.N.A. Beurskens, E. de la Luna, A. Sirinelli, M. Zerbini, and JET-EFDA contributors. Electron cyclotron emission measurements on JET: Michelson interferometer, new absolute calibration, and determination of electron temperature. *Rev. Sci. Instrum.*, 83:125101, 2012. doi:10.1063/1.4768246.

[22] M. Brix, N. C. Hawkes, A. Boboc, V. Drozdov, S. E. Sharapov, and JET-EFDA Contributors. Accuracy of EFIT equilibrium reconstruction with internal diagnostic information at JET. *Rev. Sci. Instrum.*, 79:10F325, 2008. doi:10.1063/1.2964180.

[23] T. Schreiber. Measuring information transfer. *Phys. Rev. Lett.*, 85(2):461, 2000. doi:10.1103/PhysRevLett.85.461.

[24] B.Ph. van Milligen, G. Birkenmeier, M. Ramisch, T. Estrada, C. Hidalgo, and A. Alonso. Causality detection and turbulence in fusion plasmas. *Nucl. Fusion*, 54:023011, 2014. doi:10.1088/0029-5515/54/2/023011.

[25] B.Ph. van Milligen, B.A. Carreras, L. García, A. Martin de Aguilera, C. Hidalgo, J.H. Nicolau, and the TJ-II Team. The causal relation between turbulent particle flux and density gradient. *Phys. Plasmas*, 23:072307, 2016. doi:10.1063/1.4958806.

[26] A. Jacchia, P. Mantica, F. De Luca, and G. Gorini. Determination of diffusive and nondiffusive transport in modulation experiments in plasmas. *Phys. Fluids B*, 3:3033, 1991. doi:10.1063/1.859781.

[27] J. H. Nicolau, L. García, B. A. Carreras, and B.Ph. van Milligen. Applicability of transfer entropy for the calculation of effective diffusivity in heat transport. *Phys. Plasmas*, 25:102304, 2018. doi:10.1063/1.5041495.

[28] M. Soler and J.D. Callen. On measuring the electron heat diffusion coefficient in a tokamak from sawtooth oscillation observations. *Nucl. Fusion*, 19(6):703, 1979. doi:10.1088/0029-5515/19/6/002.

[29] I. Ivanova-Stanik, L. Aho-Mantila, M. Wischmeier, R. Zagórski, and JET Contributors. COREDIV and SOLPS numerical simulations of the Nitrogen seeded JET ILW L-mode discharges. *Contrib. Plasma Phys.*, 56(6-8):760, 2016. doi:10.1002/ctpp.201610006.

[30] N. Bonanomi, P. Mantica, C. Giroud, C. Angioni, P. Manas, S. Menmuir, and JET Contributors. Light impurity transport in JET ILW L-mode plasmas. *Nucl. Fusion*, 58:036009, 2018. doi:10.1088/1741-4326/aaa4d3.

[31] C.D. Challis, J. Garcia, M. Beurskens, P. Buratti, E. Delabie, P. Drewelow, L. Frassinetti, C. Giroud, N. Hawkes, J. Hobirk, E. Joffrin, D. Keeling, D.B. King, C.F. Maggi, J. Mailloux, C. Marchetto, D. McDonald, I. Nunes, G. Pucella, S. Saarelma, J. Simpson, and JET

Contributors. Improved confinement in JET high β plasmas with an ITER-like wall. *Nucl. Fusion*, 55(5):053031, 2015. URL: `http://stacks.iop.org/0029-5515/55/i=5/a=053031`.